





Assisted metrology and preparation of macroscopic superpositions with split spin-squeezed statesJiajie Guo ¹, Fengxiao Sun ¹, Qiongyi He ^{1,2,3,*} and Matteo Fadel ^{4,†}¹*State Key Laboratory for Mesoscopic Physics, School of Physics, Frontiers Science Center for Nano-optoelectronics, & Collaborative Innovation Center of Quantum Matter, Peking University, Beijing 100871, China*²*Collaborative Innovation Center of Extreme Optics, Shanxi University, Taiyuan, Shanxi 030006, China*³*Peking University Yangtze Delta Institute of Optoelectronics, Nantong 226010, Jiangsu, China*⁴*Department of Physics, ETH Zürich, 8093 Zürich, Switzerland*

(Received 5 September 2023; accepted 30 October 2023; published 30 November 2023)

We analyze the conditional states in which one part of a split spin-squeezed state is left, upon performing a collective spin measurement on the other part. For appropriate measurement directions and outcomes, we see the possibility of obtaining states with high quantum Fisher information, even reaching the Heisenberg limit. This allows us to propose a metrological protocol that can outperform standard approaches, for example, in a situation where the number of particles in the probe is bounded. The robustness of this protocol is investigated by considering realistic forms of noise present in cold-atom experiments, such as particle number fluctuations and imperfect detection. Ultimately, we show how this measurement-based state-preparation approach can allow for the conditional (i.e., heralded) preparation of spin Schrödinger's cat states even when the initial state before splitting is only mildly squeezed.

DOI: [10.1103/PhysRevA.108.053327](https://doi.org/10.1103/PhysRevA.108.053327)**I. INTRODUCTION**

Spin-squeezed states are of paramount importance for investigating multipartite quantum correlation, as well as for quantum-enhanced metrology applications. Experimentally, these states are nowadays routinely prepared in atomic ensembles, either by controlling atomic collisions, or by light-matter interaction. In these platforms, a number of studies revealed the rich entanglement structure of spin-squeezed states [1] and demonstrated their usefulness for performing measurements with a precision surpassing the standard quantum limit [2].

Recently, the concept of split spin-squeezed states was introduced, where an ensemble of spin-squeezed particles is spatially distributed into individually addressable modes [3]. Through this process, the particle entanglement present in the initial state give origin to mode entanglement between its partitions [4], highlighting also a strong duality between these two concepts [5]. After their first experimental realization with Bose-Einstein condensates [6], split spin-squeezed states raised a lot of interest for their possible applications in quantum technologies and fundamental studies. Examples include theoretical investigations of their potential quantum metrology [7,8], recently demonstrated experimentally in [9], and for investigating multipartite quantum correlations [10–14]. Taking this successful example into consideration, it would be crucial to understand whether other quantum information tasks could be accessible by such states.

In this context, we provide here an alternative metrological protocol enabled by split spin-squeezed states. The idea is based on the fact that, due to the shared quantum correlations between the two parties of the system, performing a local measurement on one of them leaves the other in a conditional state that can have an extremely high sensitivity. This protocol can outperform the standard approach of using spin-squeezed states when the number of particles in the probe, as well as the state preparation time, are limited.

Moreover, our measurement-based state preparation protocol can result in the generation of macroscopic superposition states, also known as spin Schrödinger cat states [15,16]. In addition to their interest for metrology, such states are appealing for fundamental studies of quantum correlations in many-body systems. Their nonclassicality is notoriously related to interference fringes and negative regions in the Wigner function, which are typically difficult to prepare experimentally.

In summary, our work analyses a regime of system parameters and resources in which an assisted metrological protocol using split spin-squeezed states can offer an advantage. Moreover, we investigate the use of such states for the heralded preparations of macroscopic superposition states. These ideas could be implemented experimentally with Bose-Einstein condensates, where the preparation of cat-like spin states turned out to be extremely challenging using conventional approaches.

II. SINGLE PROBE METROLOGY WITH OAT STATES

In a typical quantum metrology scheme, the phase shift θ to be determined is encoded in a N -partite probe state ρ_0 by a generator H as $\rho = e^{-i\theta H} \rho_0 e^{i\theta H}$. A fundamental limit

*qiongyihe@pku.edu.cn

†fadelm@phys.eth.ch

to the maximum phase sensitivity is provided by the so-called quantum Cramér-Rao bound $\Delta\theta \geq \Delta\theta_{QCR} \equiv 1/\sqrt{vF_Q[\rho, H]}$, where $F_Q[\rho, H]$ is the quantum Fisher information (QFI) and v is the number of independent measurements [2]. For a pure state, the QFI can be expressed in terms of the variance of H as $F_Q[\rho, H] = 4\text{Var}[\rho, H]$. The standard quantum limit tells us that, for all classical states $F_Q[\rho, H] \leq N$, while according to the Heisenberg limit quantum states satisfy $F_Q[\rho, H] \leq N^2$. Therefore, observing $F_Q[\rho, H] > N$ implies the presence of metrologically useful entanglement [2]. Moreover, a high QFI can be related to correlations that are even stronger than entanglement, namely, Bell correlations [17].

Of paramount importance for preparing atomic ensembles in quantum states with large QFI is the one-axis twisting (OAT) dynamics [18]. Starting from an N -partite spin coherent state pointing along the $+x$ direction, the OAT Hamiltonian $H = \hbar\chi S_z^2$ gives, after an evolution time t , the state

$$|\psi(\mu)\rangle = \frac{1}{\sqrt{2^N}} \sum_{k=0}^N \sqrt{\binom{N}{k}} e^{-i\frac{\mu}{2}(N/2-k)^2} |k\rangle, \quad (1)$$

where $\mu = 2\chi t$ is an adimensional parameter and $|k\rangle$ is the Dicke state with k excitations.

The properties of state Eq. (1) have been extensively investigated theoretically [2, 19]. Notably, expectation values of the collective spin operator can be computed analytically, also for high moments [20]. This allows us to obtain analytical expressions also for the eigenvalues of the 3×3 covariance matrix $\Gamma_{ij} = \text{Cov}[S_i, S_j]$, with $S_i \in \{S_x, S_y, S_z\}$. The basis change that diagonalizes Γ is of clear physical intuition and often convenient to use. Together with the polarization direction $x = x'$, we introduce the squeezing direction $z' = -\sin\theta^*y + \cos\theta^*z$ and antisqueezing directions $y' = \cos\theta^*y + \sin\theta^*z$, with

$$\theta^* = \frac{1}{2} \arctan \left(\frac{4 \sin(\frac{\mu}{2}) \cos^{N-2}(\frac{\mu}{2})}{1 - \cos^{N-2}(\mu)} \right), \quad (2)$$

as the directions that respectively minimize (z') and maximize (y') the second moment of the collective spin.

The maximum eigenvalue of the covariance matrix Γ is also proportional to the QFI of the state Eq. (1). One obtains a QFI larger than N for $0 < \mu < 2\pi$ and even reaching N^2 for $\mu = \pi$, when a ‘‘Schödinger cat’’ state is obtained [15].

Experimentally, the OAT dynamics is implemented in, e.g., ion traps through light-mediated interactions [21] or BECs through atomic elastic collisions [22] and it is routinely used for the preparation of spin-squeezed states. These enabled numerous demonstrations of quantum-enhanced metrology, such as being applied to measuring magnetic fields [23], improving frequency resolution in atomic clocks [24, 25], and realizing squeezed matter-wave interferometry [26].

If we consider a metrological application where the number of particles in the probe is limited to some maximum number, we also set a limit to the achievable QFI (i.e., the Heisenberg limit) and thus to the sensitivity. However, one might argue that the state preparation could involve more particles than the one used in the probe itself and ask whether this could be used to provide some advantage. While it is clear that if the ancillary particles are just discarded no advantage can be

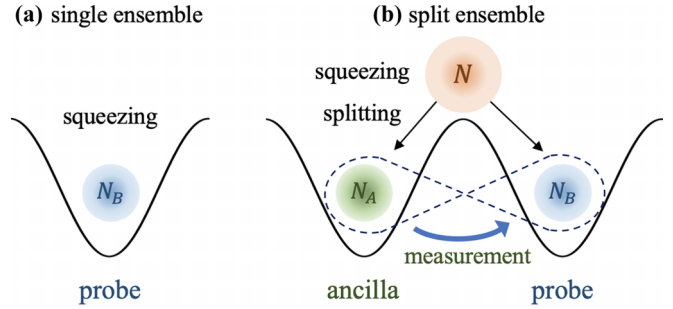


FIG. 1. State preparation and metrology with split atomic ensembles. (a) To prepare nonclassical states of many-body systems, traditional approaches rely on implementing a nonlinear dynamic in a trapped ensemble. (b) Instead, our assisted protocol is based on first spatially splitting a mildly entangled ensemble to then measure one of the two parts. Because of the shared correlations, this results in projecting the other half into a multipartite state that can have strong quantum correlations.

obtained, it is not trivial to see whether the probe sensitivity can be improved by a partial characterization of the ancillary particles’ state. Here, by partial characterization, we mean the information that can be obtained from some measurement of experimentally practical implementation, such as the result of a collective measurement performed on the ensemble of ancillary particles.

This question can be refined even further by considering a more realistic situation that includes the relevant noise sources. In fact, during the preparation of squeezed BECs there are inevitable decoherence mechanisms resulting from technical and intrinsic noise [27, 28]. The first can originate from imperfections in the implementation, while the second is fundamental as it originates from particle losses. For BECs, these noise sources limit the OAT evolution to short times ($\mu < N^{-2/3}$).

III. ASSISTED METROLOGY

To present our metrological protocol, we consider the case of an atomic ensemble in which the OAT dynamics is followed by a spatial separation of the particles into two distinct partitions [3], see Fig. 1. This last step can be realized by modifying the trapping potential to a double-well [29] or by exploiting additional internal states of the atoms [30], and it can formally be described by a beam-splitter transformation. The resulting split spin-squeezed state can thus be written as [3]

$$|\Phi(\mu)\rangle = \frac{1}{2^N} \sum_{N_A=0}^N \sum_{k_A=0}^{N_A} \sum_{k_B=0}^{N_B} \sqrt{\binom{N}{N_A} \binom{N_A}{k_A} \binom{N_B}{k_B}} \times e^{-i\frac{\mu}{2}(N/2-k_A-k_B)^2} |k_A\rangle_{N_A} |k_B\rangle_{N_B}, \quad (3)$$

where N_α is the number of particles for partition $\alpha \in \{A, B\}$ with $N_A + N_B = N$, and $|k_\alpha\rangle_{N_\alpha}$ is the N_α -particle Dicke state with k_α excitations. Crucial to this state is that the multipartite entanglement generated by the OAT dynamics is partially

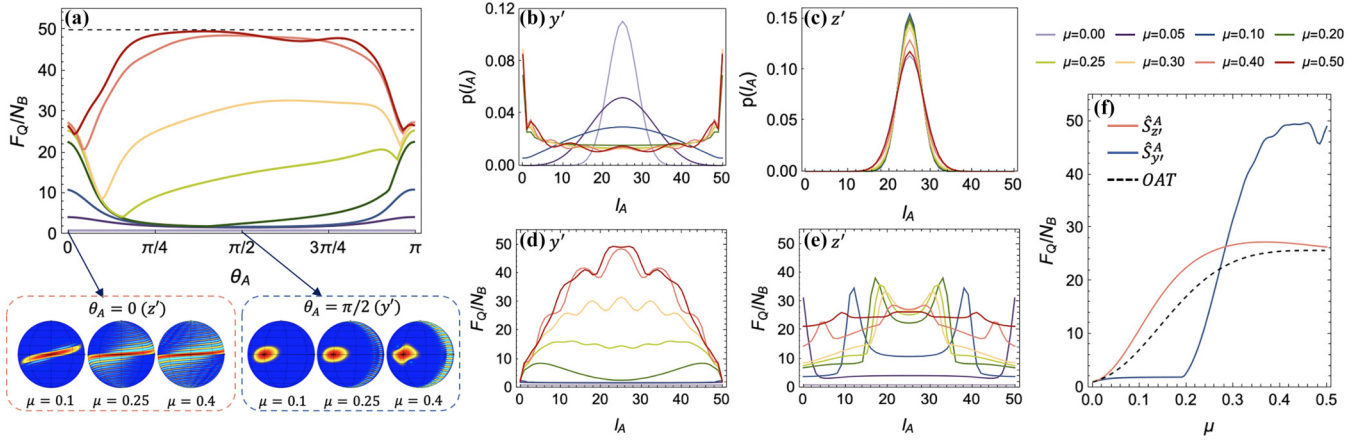


FIG. 2. Measurements on the xy plane. Properties of the conditional states obtained from a split spin-squeezed state with $N = 100$, $N_A = N_B = N/2$. (a) For $l_A = N_A/2$, F_Q/N_B as a function of the measurement direction θ_A and selected Wigner functions showing squeezed and cat-like states. Fixing θ_A such that the measurement direction is either y' or z' , we show the probability of measuring l_A , panels (b), (c) respectively, and the F_Q/N_B of the associated states, panels (d), (e). For $l_A = N_A/2$, we show in (f) a comparison between F_Q/N_B of conditional states and of OAT states, as a function of the squeezing μ . Here, the comparison is for a fixed number of particles N_B in the probe state.

“converted” by the spatial splitting into mode entanglement between the A and B partitions.

Split spin-squeezed states have already been realized experimentally [6,31], and are thus becoming relevant for practical metrological applications [9]. In the protocol we consider, N_B particles constitute the probe whose sensitivity might depends on the operations performed on the N_A ancillary particles. In the following we investigate the probe’s conditional states obtained upon performing a collective spin measurement on A and discuss in which scenarios this assisted protocol can provide a better metrological performance than the standard OAT dynamics.

A. Ideal scenario

Let us consider the situation in which it is performed a measurement of the number of ancilla particles and of their collective spin $S_{\mathbf{n}}^A$ along direction \mathbf{n} . Note that these two physical quantities can be measured simultaneously, as the associated operators commute. Obtaining as result (N_A, l_A) , the probe particles are left in the (unnormalized) state

$$|\Phi(\mu)^B\rangle = \frac{\mathbf{n}}{N_A} \langle l_A | \Phi(\mu) \rangle, \quad (4)$$

where $\frac{\mathbf{n}}{N_A} \langle l_A |$ is the N_A -particle Dicke state with l_A excitations for $S_{\mathbf{n}}^A$. The probability for this to state to occur is given by

$$p(l_A, N_A | \mathbf{n}) = \frac{1}{2^{2N}} \sum_{k_A=0}^{N_A} \sum_{k'_A=0}^{N_A} \sum_{k_B=0}^{N-N_A} \binom{N}{N_A} \binom{N-N_A}{k_B} \sqrt{\binom{N_A}{k_A} \binom{N_A}{k'_A}} e^{-i\frac{\mu}{2}(N/2-k_A-k_B)^2} e^{i\frac{\mu}{2}(N/2-k'_A-k_B)^2} \frac{\mathbf{n}}{N_A} \langle l_A | k_A \rangle_{N_A} \langle k'_A | l_A \rangle_{N_A}^{\mathbf{n}}. \quad (5)$$

This expression allows us to introduce the probability of obtaining result l_A from a measurement of $\hat{S}_{\mathbf{n}}^A$ on N_A particles, namely, $p_{N_A, \mathbf{n}}(l_A) = p(l_A, N_A | \mathbf{n})/p(N_A)$, where $p(N_\alpha) = 2^{-N} \binom{N}{N_\alpha}$ is the probability of having N_α particles in mode $\alpha \in \{A, B\}$.

For a given N_A it is worth investigating the conditional states Eq. (4), their QFI, and their probability to occur Eq. (5). From our analytical expression it is possible to consider arbitrary measurement directions \mathbf{n} and results l_A , but in the following we will focus on discussing the parameters we found most interesting.

We start considering a collective spin measurement on the yz plane performed locally on A , so that $S_{\mathbf{n}}^A = \sin \theta_A S_{y'}^A + \cos \theta_A S_{z'}^A$, where θ_A is the angle between the measurement and the squeezing direction z' . For $l_A = N_A/2$, we show in Fig. 2(a) the QFI of the conditional probe states as a function of θ_A . Interestingly, for small values of μ conditional states with large QFI are obtained for $\theta_A = 0$ (i.e., the squeezing direction z'), while for larger values of μ a large QFI is obtained for $\theta_A \approx \pi/2$ (i.e., the antisqueezing direction y'). To under-

stand better this behavior, we look at the Wigner functions of the conditional probe states resulting from different measurement angles and levels of squeezing. Interestingly, we observe that a measurement along $\theta_A \approx 0$ results in conditional states that resemble spin-squeezed and oversqueezed states, while a measurement along $\theta_A \approx \pi/2$ results in conditional states that resemble a superposition of coherent spin states, i.e., a spin cat state. To analyze the probability $p(l_A) \equiv p_{N_A, \mathbf{n}}(l_A)$ of these states to occur, we plot in Figs. 2(b) and 2(c) the value of Eq. (5) for different levels of squeezing. As μ increases, if the measurement is performed along the antisqueezing direction y' , $p(l_A)$ tends to spread uniformly over all range of l_A [see Fig. 2(b)], while for a measurement along the squeezing direction z' , then $p(l_A)$ gets peaked around $l_A = N_A/2$ [see Fig. 2(c)]. For both measurement directions, and for different results l_A , we can then compute the QFI of the conditional states, see Figs. 2(d) and 2(e).

With these in hand, we want to compare the metrological advantage given by the conditional probe states just investigated and an OAT state. The resources we keep

constrained are the number of atoms in the probe state and the adimensional squeezing parameter μ . For a nonlinearity χ independent of the particle number, the latter constraint corresponds to keeping fixed the state preparation time $t = \mu/2\chi$. In Fig. 2(f) we compare the value of F_Q/N_B for the different conditional states just discussed, with the one for an OAT state with $N_B = 50$ particles. This comparison is meaningful for a scenario where the number of particle in the probe is limited, but additional ancillary particles not interacting with the field to be estimated can be included in the state preparation and measurement. Interestingly, we see that there are situations where the conditional states reach much higher F_Q/N_B than the OAT state and that one can even saturate the Heisenberg limit, i.e., $F_Q/N_B \approx N_B$, for $\mu \ll \pi$.

In particular, when the measurement direction is aligned with the antisqueezing direction y' , we obtain for relatively large values of μ ($\mu > 0.4$ for $N_A = N_B = 50$) conditional states with F_Q/N_B that is, in general, high compared to a simple OAT state is observed. Interestingly, we also observe large fluctuations of F_Q/N_B for $\mu > 0.5$ and that it is possible to reach $F_Q/N_B \approx N_B$ for $\mu \ll \pi$ (see Supplemental Material [32], Sec. II). On the other hand, when the measurement is aligned with the squeezing direction z' , the value of F_Q/N_B obtained for the conditional states roughly follows the one for an OAT state, apart for small μ . This regime is of particular interest, as (i) these values of μ are the one typically explored in cold atom experiments, (ii) in this regime one can exceed the F_Q/N_B of an OAT state, and (iii) this occurs with high probability since $p(l_A)$ is peaked around $l_A = N_A/2$. Moreover, we will show in the following section that this configuration is also robust to noise, in the sense of particle number fluctuations and imperfect detection.

We then consider a collective spin measurement along x performed locally on A . The probability to obtain a certain measurement result l_A strongly depends on the amount of squeezing μ , Fig. 3(a). In fact, for $\mu = 0$ the state is fully polarized along x , and one has $l_A = N_A$ with unit probability, but when μ increases the state starts to “wrap around” the Bloch sphere, resulting in a nonzero probability for all possible l_A . The QFI for the associated conditional states is illustrated in Fig. 3(b), showing a large variation even reaching the Heisenberg limit. If the result $l_A = N_A$ is obtained, the conditional probe state is a mildly squeezed spin state. However, as soon as one obtains $l_A < N_A$, the resulting conditional state resembles a spin cat state, Fig. 3(c). Note that for $l_A > N_A/2$ the angular separation of the coherent spin states participating in the superposition, and therefore, also the number of interference fringes, scales with $N_A - l_A$. Moreover, remember that even if conditional states with $F_Q/N_B \approx N_B$ are possible, these occur with very small probabilities. To compare the metrological advantage given by these conditional states and an OAT state we show in Fig. 3(d) the corresponding QFI values. For relatively large values of μ ($\mu > 0.3$ for $N_A = N_B = 50$) we obtain conditional states with F_Q/N_B that strongly fluctuates, taking values both larger and lower than the one of an OAT state. The behavior is much more regular for small values of μ , where we can see a regime in which conditional states with $l_A < N_A$ give a F_Q/N_B growing in time much faster than the one of an OAT state[see $\mu < 0.1$ in Fig. 3(d)]. This regime is the one

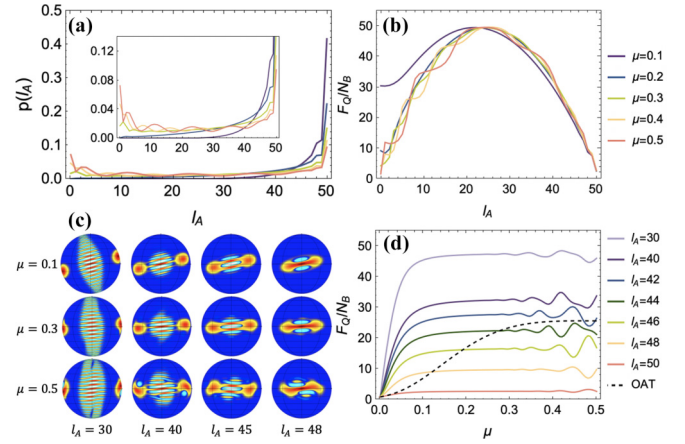


FIG. 3. Measurements along the x direction. Properties of the conditional states obtained from a split spin-squeezed state with $N = 100$, $N_A = N_B = N/2$. (a) Probability of measuring l_A for different levels of squeezing and (b) the F_Q/N_B of the associated conditional states. (c) Selected Wigner functions showing cat-like states of different size. (d) Comparison between F_Q/N_B of conditional states and of OAT states, as a function of the squeezing μ . Here, the comparison is for a fixed number of particles N_B in the probe state.

resulting in conditional states that closely resemble spin cat states.

In Sec. I of the Supplemental Material [32] we give more details about the states considered so far, while in Sec. II of [32] we show Wigner functions of the conditional states resulting from several other measurement directions and outcomes, together with their properties.

B. Noisy scenarios

So far we considered a fixed N_A , but the splitting process resulting in the state Eq. (3) is associated to partition noise which makes N_A and $N_B = N - N_A$ fluctuate. For the equal (50:50) splitting we considered, the probability to observe N_α particles in mode $\alpha = A, B$ is simply given by the Binomial distribution $p(N_\alpha)$. Concretely, this means that in an experiment the probe states will have a fluctuating number of particles and, therefore, a fluctuating sensitivity. In a practical scenario it would be extremely inefficient to postselect only experimental realisations with a given N_B , therefore, we might ask what is the average sensitivity if all realizations are considered. In each realization, A 's measurement gives knowledge of N_A and l_A , which would allow us to perform a local optimization on the B side to exploit the maximum sensitivity of the conditional state. We can thus define the average QFI density as

$$\left\langle \frac{F_Q}{N_B} \right\rangle_{l_A} = \sum_{N_B=0}^N p(N_B) \frac{F_Q[\rho_{l_A, N_A}^B | \mathbf{n}]}{N_B}, \quad (6)$$

where $F_B[\rho_{l_A, N_A}^B | \mathbf{n}]$ is the QFI of the conditional probe state $\rho_{l_A, N_A}^B | \mathbf{n}$. This last term is obtained from a measurement on A along the direction specified by \mathbf{n} and giving as result l_A . However, note that l_A has now to be a function of N_A since the size of system A is fluctuating. For example, we could compute Eq. (6) for the case when $l_A = [N_A/2]$, which we

have seen to be the most likely result for measurements on the yz plane and small μ , see Figs. 2(b) and 2(c). Remarkably, we observe that there is no appreciable difference between a numerical evaluation of $\langle F_Q/N_B \rangle$ for measurements on the yz plane and $l_A = \lceil N_A/2 \rceil$ and the value of F_Q/N_B when $N_A = N_B = N/2$ and $l_A = N_A/2$. In other words, averaging F_Q/N_B over the distribution $p(N_B)$ seems to give a result compatible with the value of F_Q/N_B when $N_B = N/2$. This could be explained by noting that (i) for large N the distribution $p(N_B)$ is sharply peaked and symmetric around $N_B = N/2$, and (ii) in the averaging, the F_Q/N_B of a state with $N_B = N/2 + k$ particles compensates the one of a state with $N_B = N/2 - k$ particles, resulting in a value very close to the F_Q/N_B of a state with $N_B = N/2$ particles. Perhaps surprisingly, we find that this correspondence holds for any value of μ , and for different choices of the function for l_A (e.g., $l_A = N_A - 1$ for measurements of S_x^A). More details about this comparison can be found in Sec. II B of the Supplemental Material [32]. There, we also compare another possible definition of average QFI in the case where no measurement optimisation is done on the B side depending on the value of N_B [still, the same postselection according to $l_A(N_A)$ is applied]. Even in this scenario, we observe that the average QFI is compatible with the value of F_Q/N_B when $N_B = N/2$, which can be attributed to the fact that conditional states with different $N_B \approx N/2$ can appear very similar.

The second type of noise that we analyze is a measurement noise that results in errors on the observed value of l_A . Experimentally, this can originate from imperfect atom number counting, which always happens as detectors have finite resolution. We model this noise as a Gaussian distribution centered around l_A and of standard deviation σ , such that if the value l_A^* is observed there is a probability $p_{l_A, \sigma}(l_A^*) = (2\pi\sigma^2)^{-1/2} e^{-l_A^* - l_A)^2 / 2\sigma^2}$ for the true value to be l_A .

Analogously to the previous case, we define the QFI averaged over different values of l_A as

$$\left\langle \frac{F_Q}{N_B} \right\rangle_{l_A^*} = \frac{F_Q \left[\mathcal{N} \sum_{l_A=0}^{N_A} p_{N_A, n}(l_A) p_{l_A, \sigma}(l_A^*) \rho_{l_A, N_A, n}^B \right]}{N_B}, \quad (7)$$

where $\mathcal{N}^{-1} = \sum_{l_A=0}^{N_A} p_{N_A, n}(l_A) p_{l_A, \sigma}(l_A^*)$ is a normalization parameter. We illustrate in Fig. 4 how this quantity varies as a function of σ , and for different measurement settings on A .

Figure 4(a) shows that the noise we are considering affects differently the conditional states obtained upon measurement of S_y^A or S_z^A . In the first case, it appears that there exists a critical level of noise σ^* after which the average QFI is the one of a mixture of coherent spin states. On the other hand, this is not true in the second case, where we see the average QFI decreasing only asymptotically. We can understand this behavior by looking at the Wigners in Fig. 2(a), where it is reasonable to expect that the Gaussian-like conditional states resulting from S_z^A measurements are more robust than the cat-like conditional states resulting from S_y^A measurements. For a given amount of noise σ , it is interesting to know how the average QFI changes as a function of the squeezing μ . This is illustrated in Fig. 4(b), for different levels of noise σ . Interestingly, while the fragility of the conditional states obtained from S_y^A measurements results in an average QFI that can quickly fall below the value of the QFI for an OAT

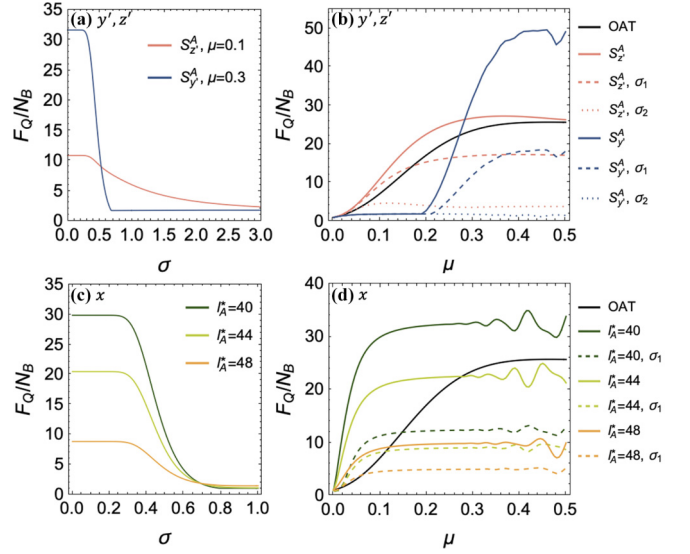


FIG. 4. Robustness to detection noise. Sensitivity of the conditional states obtained from a split spin-squeezed state with $N = 100$, $N_A = N_B = N/2$. Panels (a), (b) consider conditional states with $l_A^* = N_A/2$ resulting from measurements along y' and z' , while panels (c), (d) along x . Panels (a), (c) show F_Q/N_B as a function of the detection noise σ , while (b), (d) as a function of the squeezing μ . Dashed lines are for a level of noise $\sigma_1 = 0.49$, while dotted lines for $\sigma_2 = 1.37$, which correspond to a 10% probability of having $l_A = l_A^* \pm 1$ or $l_A = l_A^* \pm 2$, respectively.

state, conditional states obtained from S_z^A measurements seem able to achieve an average QFI larger than the one of an OAT state for small μ , even if σ is relatively large. This result further supports the statement made in the previous section, saying that the regime of small μ and S_z^A measurements is of great interest for assisted metrology tasks since it results in conditional states with high sensitivity and noise robustness.

Figure 4(c) shows how the measurement noise we are considering affects the conditional states obtained upon measurement of S_x^A , for different values of the result l_A^* . As expected, the average QFI of conditional states with larger l_A^* decays faster as the noise σ increases since such states are cat-like states with fine structures in the Wigner function that are rapidly washed-out by noise, see Fig. 3(c). Also in this scenario, it is interesting to know how the average QFI changes as a function of the squeezing μ for a fixed amount of noise σ . This is illustrated in Fig. 4(d), for conditional states with different l_A^* . For small values of μ it is possible to see that the QFI of a state can be surpassed by the considered conditional states, given a $l_A^* < N$ and a small enough σ .

In addition, a further analysis on imperfection on atom counting on both N_α and l_A is discussed in the Supplemental Material [32], Sec. III.

IV. MEASUREMENT-BASED PREPARATION OF SPIN CAT STATES

Schrödinger cat states are regarded as powerful resources for quantum metrology, error-corrected quantum computing, and fundamental studies. While cat states have been successfully implemented with trapped ions [33,34], Rydberg atoms

[35], optical and microwave photons [36–40], and mechanical oscillators [41], their realization atomic ensembles has remained elusive. Difficulties lie in engineering the correct nonlinear interactions, suppressing noise mechanisms (such as particle losses and phase noise), and performing measurements with high resolution.

It is known that the OAT dynamics Eq. (1) result in a spin cat state at $\mu = \pi$ [15]. Nevertheless, following this simple strategy is unrealistic for BECs due to the severe particle losses that would occur during the long dynamics. Approaches to mitigate these have been investigated [16], even if their experimental implementation remains challenging. Alternatively, ideas have been proposed to prepare macroscopic superpositions between two modes of a spin-1 BEC with a dynamic governed by spin-exchanging collisions [42].

In the analysis of conditional states we presented, we have seen that spin cat states can be obtained as a result of measurement along suitable directions (e.g., S_y^A or S_x^A), if the appropriate results are obtained, see Figs. 2 and 3. We can thus propose to use this approach for the heralded preparation of macroscopic superposition states in spin-1/2 BECs. Crucially, even if this protocol demands a high resolution in counting the number of particles, it has the advantage of being potentially fast, as the initial squeezed state that needs to be prepared requires an OAT evolution parameter μ much smaller than π for S_x^A measurements, see Fig. 3.

To understand the robustness of the protocol we propose, we investigate how finite measurement resolution affects the prepared state. From Figs. 3 and 5 we can see that after a measurement of S_x^A different cat states are obtained depending on the result l_A . In particular, these states have different size (i.e., separation between the two coherent spin state components), different parity (i.e., Wigner function value at the origin), and different orientation on the yz plane. Therefore, if in an experiment the measured l_A^* differs from the actual l_A because of noise, the resulting conditional state will be a statistical mixture of different cat states. If this noise is too large, averaging over different cat states would result in a washing-out of the interference fringes and thus of the quantum coherence of the superposition. Importantly, to estimate what is the amount of noise that can be tolerated it is not enough to take into account the variance σ^2 of the Gaussian distribution modeling uncertainties in l_A , but also the probability that a certain l_A occurs for the parameters considered (see Eq. (5) of the Supplemental Material [32]). For this reason, if result l_A^* is obtained, the conditional mixed state takes the form

$$\rho(l_A^*, \sigma) = \mathcal{N} \sum_{l_A=0}^{N_A} p_{N_A, \delta_n^A}(l_A) p_{l_A, \sigma}(l_A^*) \rho_{l_A, N_A}^B. \quad (8)$$

In Fig. 5(a) we plot the Wigner function of such states for different values of l_A^* and σ . Even if the precise value of the noise that can be tolerated depends on the l_A^* considered, we observe that around $\sigma \approx 0.7$ the interference fringes characterising the coherent superposition vanish. This value corresponds to an approximate probability of $p \approx 0.2$ for the real value of l_A to be $l_A^* \pm 1$.

A more quantitative analysis of the effect of noise is obtained by looking at the negativity of the Wigner function. For continuous variable systems, Wigner negativity is related to

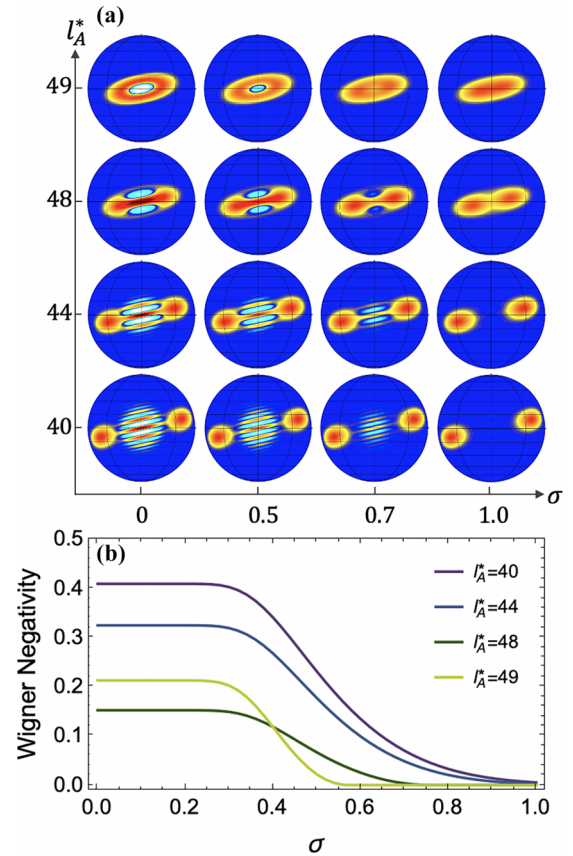


FIG. 5. Heralded generation of cat states. Nonclassical features of the conditional states obtained from a split spin-squeezed state with $N = 100$, $N_A = N_B = N/2$, after measuring S_x^A . We show, as a function of the level of detection noise σ . (a) Wigner functions of conditional states associated to different l_A^* and (b) Wigner function negativity as defined in Eq. (9).

the non-Gaussianity and nonclassicality of the state [43] and it is known to be a resource for quantum information tasks [44–46]. For spin systems, however, the Wigner function is defined on a (generalized Bloch) sphere and the definition of non-Gaussianity and negativity is subtle. Here we follow Ref. [47] and compute the Wigner negativity as

$$WN(\rho) = \frac{1}{2} \left(\frac{2j+1}{4\pi} \int_{\theta=0}^{\pi} \int_{\phi=0}^{2\pi} |W_\rho(\theta, \phi)| \sin \theta d\theta d\phi - 1 \right), \quad (9)$$

where $W_\rho(\theta, \phi)$ is the value of the Wigner function at point (θ, ϕ) on the Bloch sphere, see Sec. IV of the Supplemental Material [32]. In Fig. 5(b) we show how the negativity of the conditional mixed states' Wigner function changes as a function of the amount of noise σ , for different values of l_A^* . For small σ , we have that ρ stays very close to a pure state with $l_A^* \approx l_A$, so that its negativity stays constant until a critical value of σ [approximately 0.4 in Fig. 5(b)] where conditional states with $l_A^* \pm 1$ start to contribute. After this point the negativity decreases until the point where it completely vanishes [approximately 0.5–0.9 in Fig. 5(b)].

V. CONCLUSION

We analyzed the conditional states resulting from a local measurement in one of the two parts of a split-spin squeezed state. The multipartite entanglement present in these states, combined with the local measurement, leads to a rich family of nontrivial conditional states exhibiting high Fisher information or large Wigner negativities. These were investigated quantitatively, for different local measurement directions and outcomes, both without and with the presence of noise. The latter was chosen to take into account particle number fluctuations in the conditional states, which are intrinsic in the probabilistic (beam-splitter-like) splitting process, as well as measurement imperfections. We observe that the observed nonclassical properties are robust to noise, and therefore of interest for applications in quantum technologies.

In this context, we propose a protocol that can be used to enhance the sensitivity of a measurement probe in a scenario where its size, as well as the state preparation time, are limited. Our idea is based on the fact that, if the probe is entangled with an ancilla system, a local measurement in the latter can prepare the probe in conditional states with much higher sensitivity. Concretely, we analyze a scenario where a split spin-squeezed state is shared between the probe and the ancilla and identified the range of system parameters and local measurements providing a metrological advantage.

In addition this practical application, we note that the measurement-based state preparation protocol we investigate

can be used to generate spin cat states. These macroscopic superposition states are of interest not only for metrology, but also for fundamental research. We quantify the nonclassicality of the conditional states that can be prepared through a measure of their Wigner function negativity and investigated its robustness with noise.

A natural platform where our ideas could be realized are ultracold atomic ensembles, where spin-squeezed states are routinely prepared for a number of applications. More recently, the spatial splitting of such states was also demonstrated [6,31], thus opening the path to the experimental study of split spin-squeezed states [3]. Apart from shedding light on multipartite quantum correlations [10–12], it is of interest to investigate the usefulness of such states for quantum technologies, such as for quantum teleportation [48] and metrology [7,8]. Our study brings a contribution in these interesting directions.

ACKNOWLEDGMENTS

This work is supported by the National Natural Science Foundation of China (Grants No. 12125402, No. 11975026, and No. 12147148) and the Beijing Natural Science Foundation (Z190005). J.G. acknowledges financial support from the China Scholarship Council (Grant No. 202106010192). FS acknowledges the China Postdoctoral Science Foundation (Grant No. 2020M680186). M.F. was supported by The Branco Weiss Fellowship–Society in Science, administered by the ETH Zürich.

-
- [1] I. Frérot, M. Fadel, and M. Lewenstein, *Rep. Prog. Phys.* **86**, 114001 (2023).
 - [2] L. Pezzè, A. Smerzi, M. K. Oberthaler, R. Schmied, and P. Treutlein, *Rev. Mod. Phys.* **90**, 035005 (2018).
 - [3] Y. Jing, M. Fadel, V. Ivannikov, and T. Byrnes, *New J. Phys.* **21**, 093038 (2019).
 - [4] N. Killoran, M. Cramer, and M. B. Plenio, *Phys. Rev. Lett.* **112**, 150501 (2014).
 - [5] M. Fadel and M. Gessner, *Phys. Rev. A* **102**, 012412 (2020).
 - [6] M. Fadel, T. Zibold, B. Décamps, and P. Treutlein, *Science* **360**, 409 (2018).
 - [7] M. Fadel, B. Yadin, Y. Mao, T. Byrnes, and M. Gessner, *New J. Phys.* **25**, 073006 (2023).
 - [8] J. Guo, F.-X. Sun, D. Zhu, M. Gessner, Q. He, and M. Fadel, *Phys. Rev. A* **108**, 012435 (2023).
 - [9] B. K. Malia, Y. Wu, J. Martínez-Rincón, and M. A. Kasevich, *Nature (London)* **612**, 661 (2022).
 - [10] B. Morris, B. Yadin, M. Fadel, T. Zibold, P. Treutlein, and G. Adesso, *Phys. Rev. X* **10**, 041012 (2020).
 - [11] M. Fadel, A. Usui, M. Huber, N. Friis, and G. Vitagliano, *Phys. Rev. Lett.* **127**, 010401 (2021).
 - [12] J. Kitzinger, X. Meng, M. Fadel, V. Ivannikov, K. Nemoto, W. J. Munro, and T. Byrnes, *Phys. Rev. A* **104**, 043323 (2021).
 - [13] G. Vitagliano, M. Fadel, I. Apellaniz, M. Kleinmann, B. Lücke, C. Klempt, and G. Tóth, *Quantum* **7**, 914 (2023).
 - [14] M. Fadel, L. Ares, A. Luis, and Q. He, *Phys. Rev. A* **101**, 052117 (2020).
 - [15] K. Mølmer and A. Sørensen, *Phys. Rev. Lett.* **82**, 1835 (1999).
 - [16] K. Pawłowski, M. Fadel, P. Treutlein, Y. Castin, and A. Sinatra, *Phys. Rev. A* **95**, 063609 (2017).
 - [17] F. Fröwis, M. Fadel, P. Treutlein, N. Gisin, and N. Brunner, *Phys. Rev. A* **99**, 040101(R) (2019).
 - [18] M. Kitagawa and M. Ueda, *Phys. Rev. A* **47**, 5138 (1993).
 - [19] J. Ma, X. Wang, C. Sun, and F. Nori, *Phys. Rep.* **509**, 89 (2011).
 - [20] J. Guo, J. Tura, Q. He, and M. Fadel, *Phys. Rev. Lett.* **131**, 070201 (2023).
 - [21] J. G. Bohnet, B. C. Sawyer, J. W. Britton, M. L. Wall, A. M. Rey, M. Foss-Feig, and J. J. Bollinger, *Science* **352**, 1297 (2016).
 - [22] M. F. Riedel, P. Böhi, Y. Li, T. W. Hänsch, A. Sinatra, and P. Treutlein, *Nature (London)* **464**, 1170 (2010).
 - [23] C. F. Ockeloen, R. Schmied, M. F. Riedel, and P. Treutlein, *Phys. Rev. Lett.* **111**, 143001 (2013).
 - [24] A. D. Ludlow, M. M. Boyd, J. Ye, E. Peik, and P. O. Schmidt, *Rev. Mod. Phys.* **87**, 637 (2015).
 - [25] E. Pedrozo-Peñafiel, S. Colombo, C. Shu, A. F. Adiyatullin, Z. Li, E. Mendez, B. Braverman, A. Kawasaki, D. Akamatsu, Y. Xiao, and V. Vuletić, *Nature (London)* **588**, 414 (2020).
 - [26] G. P. Greve, C. Luo, B. Wu, and J. K. Thompson, *Nature (London)* **610**, 472 (2022).
 - [27] Y. Li, P. Treutlein, J. Reichel, and A. Sinatra, *Eur. Phys. J. B* **68**, 365 (2009).
 - [28] Y. Li, K. Pawłowski, B. Décamps, P. Colciaghi, M. Fadel, P. Treutlein, and T. Zibold, *Phys. Rev. Lett.* **125**, 123402 (2020).

- [29] M. Fadel, *Many-Particle Entanglement, Einstein-Podolsky-Rosen Steering and Bell Correlations in Bose-Einstein Condensates* (Springer International, New York, 2022).
- [30] P. Kunkel, M. Prüfer, S. Lannig, R. Rosa-Medina, A. Bonnin, M. Gärtner, H. Strobel, and M. K. Oberthaler, *Phys. Rev. Lett.* **123**, 063603 (2019).
- [31] P. Colciaghi, Y. Li, P. Treutlein, and T. Zibold, *Phys. Rev. X* **13**, 021031 (2023).
- [32] See Supplemental Material at <http://link.aps.org/supplemental/10.1103/PhysRevA.108.053327> for an introduction of one-axis twisting dynamics and quantum Fisher information, a detailed analysis of conditional states, noise on the local atom number, and Wigner negativity for spin states, which includes Refs. [49,50].
- [33] C. Monroe, D. M. Meekhof, B. E. King, and D. J. Wineland, *Science* **272**, 1131 (1996).
- [34] H.-Y. Lo, D. Kienzler, L. de Clercq, M. Marinelli, V. Negnevitsky, B. C. Keitch, and J. P. Home, *Nature (London)* **521**, 336 (2015).
- [35] A. Omran, H. Levine, A. Keesling, G. Semeghini, T. T. Wang, S. Ebadi, H. Bernien, A. S. Zibrov, H. Pichler, S. Choi, J. Cui, M. Rossignolo, P. Rembold, S. Montangero, T. Calarco, M. Endres, M. Greiner, V. Vuletić, and M. D. Lukin, *Science* **365**, 570 (2019).
- [36] A. Ourjoumtsev, H. Jeong, R. Tualle-Brouiri, and P. Grangier, *Nature (London)* **448**, 784 (2007).
- [37] K. Huang, H. Le Jeannic, J. Ruaudel, V. B. Verma, M. D. Shaw, F. Marsili, S. W. Nam, E. Wu, H. Zeng, Y.-C. Jeong, R. Filip, O. Morin, and J. Laurat, *Phys. Rev. Lett.* **115**, 023602 (2015).
- [38] A. Auffeves, P. Maioli, T. Meunier, S. Gleyzes, G. Nogues, M. Brune, J. M. Raimond, and S. Haroche, *Phys. Rev. Lett.* **91**, 230405 (2003).
- [39] S. Deléglise, I. Dotsenko, C. Sayrin, J. Bernu, M. Brune, J.-M. Raimond, and S. Haroche, *Nature (London)* **455**, 510 (2008).
- [40] B. Vlastakis, G. Kirchmair, Z. Leghtas, S. E. Nigg, L. Frunzio, S. M. Girvin, M. Mirrahimi, M. H. Devoret, and R. J. Schoelkopf, *Science* **342**, 607 (2013).
- [41] M. Bild, M. Fadel, Y. Yang, U. von Lüpke, P. Martin, A. Bruno, and Y. Chu, *Science* **380**, 274 (2023).
- [42] L. Pezzè, M. Gessner, P. Feldmann, C. Klempt, L. Santos, and A. Smerzi, *Phys. Rev. Lett.* **123**, 260403 (2019).
- [43] A. Kenfack and K. Życzkowski, *J. Opt. B: Quantum Semiclass. Opt.* **6**, 396 (2004).
- [44] R. Takagi and Q. Zhuang, *Phys. Rev. A* **97**, 062337 (2018).
- [45] F. Albarelli, M. G. Genoni, M. G. A. Paris, and A. Ferraro, *Phys. Rev. A* **98**, 052350 (2018).
- [46] A. Mari and J. Eisert, *Phys. Rev. Lett.* **109**, 230503 (2012).
- [47] J. Davis, M. Kumari, R. B. Mann, and S. Ghose, *Phys. Rev. Res.* **3**, 033134 (2021).
- [48] M. Chaudhary, M. Fadel, E. O. Ilo-Okeke, A. N. Pyrkov, V. Ivannikov, and T. Byrnes, *Phys. Rev. A* **103**, 062417 (2021).
- [49] J. P. Dowling, G. S. Agarwal, and W. P. Schleich, *Phys. Rev. A* **49**, 4101 (1994).
- [50] T. Byrnes and E. O. Ilo-Okeke, *Quantum Atom Optics: Theory and Applications to Quantum Technology* (Cambridge University Press, Cambridge, England, 2021).